

# Optimized Detection with Analog Beamforming for Monostatic Integrated Sensing and Communication

Rodrigo Hernangómez\*, Jochen Fink\*, Renato L.G. Cavalcante\*, Zoran Utkovski\*, Sławomir Stańczak\*<sup>†</sup>

\*Fraunhofer Heinrich Hertz Institute, Germany, {firstname.lastname}@hhi.fraunhofer.de

<sup>†</sup>Network Information Theory Group, Technische Universität Berlin, Germany

**Abstract**—In this paper, we formalize an optimization framework for analog beamforming in the context of monostatic integrated sensing and communication (ISAC), where we also address the problem of self-interference in the analog domain. As a result, we derive semidefinite programs to approach detection-optimal transmit and receive beamformers, and we devise a superiorized iterative projection algorithm to approximate them. Our simulations show that this approach outperforms the detection performance of well-known design techniques for ISAC beamforming, while it achieves satisfactory self-interference suppression.

**Index Terms**—Integrated sensing and communication, beamforming, self-interference suppression, target detection, projections onto convex sets.

## I. INTRODUCTION

Integrated sensing and communication (ISAC) has been identified as one key component of next-generation mobile networks, with application areas ranging from health and smart homes to vehicular networks and industry [1]. Indeed, the current trend to automatize industrial and automotive systems often leads to a growing number of radiofrequency hardware and software components to satisfy their sensing and communication needs. In this context, the development of small-form-factor and cost-efficient ISAC solutions is particularly interesting to temper down the increased cost, size, and energy consumption that the added functionalities may bring along.

Monostatic ISAC, i.e., with co-located transmission (TX) and reception (RX) antennas, emerges as the best modality from those discussed in the literature to achieve a compact and efficient integration in standalone devices. Here, the inherent synchronization between TX and RX and the full knowledge of the transmitted signal are seen as its main advantages against the bistatic counterpart [1, 2]. On the other hand, the desired continuous transmission of data rules out pulse radar techniques and gives rise to self-interference (SI), which hampers monostatic sensing.

A strong self-interference requires the cancellation of the unwanted signal via digital signal processing techniques, such as moving target indication or adaptive filtering. Moreover, the presence of self-interference can also cause problems to the analog circuits, e.g., RX-amplifier saturation or an insufficient dynamic range at the analog-to-digital converter (ADC) [3]. Practical systems, typically based on orthogonal frequency-

division multiplexing (OFDM) in the millimeter-wave band [4, 5], often circumvent self-interference through a moderate TX-RX separation ( $\approx 50$  cm). Nevertheless, this leads to physically large devices that may be unpractical in the mentioned setups.

As an alternative to suppress self-interference, full-duplex communication schemes [3] have recently inspired the exploration of beamforming in its different architectures: digital [6], hybrid [2], or analog [7]. Specifically, Liu et al. [7] design TX and RX analog beamformers such that the self-interference is projected into their null space while allocating beams for sensing and communication. In doing so, the goal is to reduce the sidelobe level (SLL).

Analog beamforming is particularly interesting due to its ability to address self-interference in the analog domain without dedicated canceller circuits [2, 6, 7]; however, it comes at the expense of not being able to estimate the angle via array-processing algorithms, such as multiple signal classification (MUSIC) [1]. Against this background, we have identified angle-selective target detection as the key performance indicator of analog-beamforming design for sensing. Thus, we build upon the heuristic method in [7] to formalize a framework for optimal detection given the constraints imposed by communication, self-interference, and power. We propose parallel TX and RX optimization to approximate the optimal solution using a superiorized projection algorithm. This technique, which has been previously applied to wireless problems such as MIMO detection [8] or multicast beamforming [9, 10], follows the superiorization principle [11] by adding bounded perturbations to an iterative projection algorithm [12]. Simulations show that our framework outperforms the popular technique of mean squared error (MSE) minimization [13–16].

In the remainder of this section, we introduce the notation and our system model. We formalize the optimization problem for analog-beamforming ISAC detection in Section II, for which we derive parallel TX/RX problems that we approximate via superiorized projections onto convex sets. We deliver numerical results in Section III, and a conclusion in Section IV.

### A. Notation and Preliminaries

In the following, lower case letters  $a$  denote scalars, bold lower case letters  $\mathbf{x}$  denote column vectors, and bold upper case letters  $\mathbf{X}$  denote matrices. We write the complex conjugate of a scalar  $z \in \mathbb{C}$  as  $z^*$ , the transpose of a vector or matrix  $\mathbf{X}$  as  $\mathbf{X}^T$ , and its Hermitian transpose as  $\mathbf{X}^H$ . We denote by

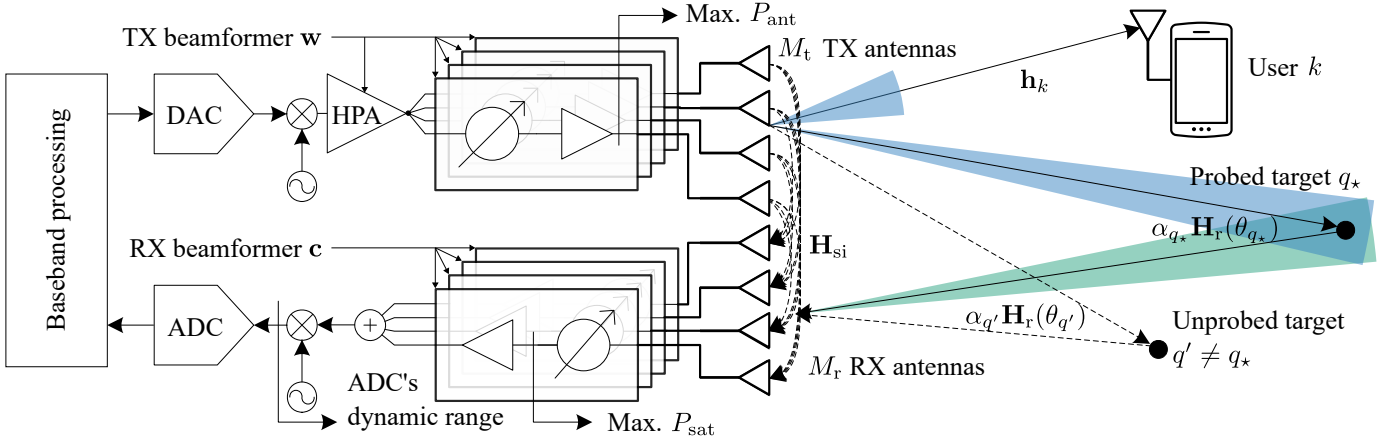


Fig. 1: System model of a monostatic ISAC transceiver with analog beamforming.

$\mathbf{I}$ ,  $\mathbf{0}$  and  $\mathbf{e}_m$  the identity matrix, zero matrix, and the  $m$ th Cartesian unit vector, respectively, where the dimensions will be clear from the context. We write  $(\forall \mathbf{x} \in \mathbb{C}^N) \|\mathbf{x}\| := \sqrt{\mathbf{x}^H \mathbf{x}}$  for the Euclidean norm of  $\mathbf{x}$ , and  $\mathbb{E}[X]$  for the expected value of a random variable  $X$ . We also write  $\mathbb{R}_+ := (0, \infty)$  for the set of the positive real numbers,  $\delta := \mathbb{Z} \rightarrow \{0, 1\}$  for the Kronecker delta with  $\delta(n) = 1$  if  $n = 0$  and  $\delta(n) = 0$  otherwise, and  $\mathbf{X} \succeq \mathbf{0}$  for positive semidefinite matrices  $\mathbf{X}$ . We use the shortcuts  $[N] := \{1, \dots, N\}$  for positive index sets with  $N \in \mathbb{N}$ , and  $\mathbb{V} \subseteq [-\pi, \pi)$  for the visible region of an antenna array.

For any closed convex set  $\mathcal{C}$  in a Hilbert space  $(\mathcal{H}, \langle \cdot, \cdot \rangle)$ , we denote by  $P_{\mathcal{C}}(\mathbf{X})$  the projection of  $\mathbf{X} \in \mathcal{H}$  onto  $\mathcal{C}$ , and by  $(\forall \mathbf{X} \in \mathcal{H}) T_{\mathcal{C}}^{\mu}(\mathbf{X}) := \mathbf{X} + \mu(P_{\mathcal{C}}(\mathbf{X}) - \mathbf{X})$  the relaxed projection onto  $\mathcal{C}$  with a relaxation parameter  $\mu \in (0, 2)$ . Additionally, we use the shortcut  $(\forall l \in [L], \forall \mathcal{C}_l \subset \mathcal{H}) T_{\mathcal{C}_{L-1}}^{\mu}(\mathbf{X}) := T_{\mathcal{C}_L}^{\mu} \dots T_{\mathcal{C}_1}^{\mu}(\mathbf{X})$ . Throughout this paper, we consider the *real* Hilbert space of Hermitian matrices,  $\mathcal{H} = \mathbb{H}^M := \{\mathbf{X} \in \mathbb{C}^{M \times M} | \mathbf{X} = \mathbf{X}^H\}$  with the trace inner product  $\langle \mathbf{A}, \mathbf{B} \rangle := \text{tr}(\mathbf{B}^H \mathbf{A}) = \text{tr}(\mathbf{B} \mathbf{A}) \in \mathbb{R}$ , which induces the Frobenius norm  $(\forall \mathbf{X} \in \mathcal{H}) \|\mathbf{X}\|_{\mathcal{H}} := \sqrt{\langle \mathbf{X}, \mathbf{X} \rangle}$ .

### B. System Model

The system model is depicted in Fig. 1. It consists of an ISAC transceiver with  $M_t$  and  $M_r$  antennas for TX and RX and individual phase and gain control. The TX beamformer  $\mathbf{w} \in \mathbb{C}^{M_t \times 1}$  is not normalized to account for the TX power  $P_t := \|\mathbf{w}\|^2$ , while the RX beamformer  $\mathbf{c} \in \mathbb{C}^{M_r \times 1}$  fulfills  $\|\mathbf{c}\| = 1$ . Each TX antenna has a maximum output power,  $P_{\text{ant}}$ , and each RX antenna has a saturation power,  $P_{\text{sat}}$ .

At a given time slot of duration  $T$ , the ISAC transceiver produces a narrowband baseband signal  $(\forall n \in [N]) s(n) \in \mathbb{C}$  with i.i.d. samples and unit average power, e.g.:

$$(\forall n \in [N]) \quad \mathbb{E}[|s(n)|^2] = 1. \quad (1)$$

Under (1), the antenna covariances can be computed as  $\mathbf{W} := \mathbf{w}\mathbf{w}^H$  and  $\mathbf{C} := \mathbf{c}\mathbf{c}^H$  [14]. The signal is transmitted over a carrier frequency  $f_0$  to serve multiplexed data to  $K$  users. For this, a bandwidth  $B_k$  is allocated to each user so that

the total bandwidth  $B_s := \sum_{k \in [K]} B_k < N/T \ll f_0$ . After reception and demodulation, each user obtains  $(\forall k \in [K]) y_k(n) = \bar{y}_k(n) + w_k(n)$ , where  $\bar{y}_k(n) := \mathbf{h}_k^H \mathbf{w} s(n)$ ,  $\mathbf{h}_k \in \mathbb{C}^{M_t \times 1}$  is the MIMO channel for user  $k$ , and  $(\forall n \in [N]) w_k(n) \sim \mathcal{CN}(0, \sigma_k^2)$  circularly-symmetric complex white Gaussian noise. Each user  $k$  requires a certain rate  $R_k$  that is achieved by meeting a minimum signal-to-noise ratio (SNR)  $\Gamma_k$   $(\forall k \in [K])$ :

$$\frac{\mathbb{E}[|\bar{y}_k(n)|^2]}{\mathbb{E}[|w_k(n)|^2]} = \frac{|\mathbf{h}_k^H \mathbf{w}|^2}{\sigma_k^2} \geq \Gamma_k = 2^{R_k/B_k} - 1. \quad (2)$$

*Integrated Sensing and Communication:* The ISAC transceiver also receives  $s(n)$  via the backscatter and SI channels with the impulse responses given by  $(\forall n \in [N]) \bar{\mathbf{H}}_r(n), \bar{\mathbf{H}}_{\text{si}}(n) \in \mathbb{C}^{M_r \times M_t}$ , respectively.  $\bar{\mathbf{H}}_r(n)$  originates from  $Q$  targets, each one characterized by the tuple  $(\xi_q, r_q, \theta_q) \in \mathbb{R}_+ \times \mathbb{R}_+ \times \mathbb{V}$  representing the radar cross section, the distance to the transceiver, and the direction of arrival:

$$\bar{\mathbf{H}}_r(n) = \sum_{q \in [Q]} \alpha_q \mathbf{H}_r(\theta_q) \delta(n - n_q), \quad n_q := \frac{2Nr_q}{Tc}, \quad (3a)$$

$$\mathbf{H}_r(\theta_q) = \mathbf{a}_{M_r}(\theta_q) \mathbf{a}_{M_t}^H(\theta_q), \quad \alpha_q = \sqrt{\frac{\xi_q \lambda^2}{(4\pi)^3 r_q^4}}. \quad (3b)$$

Here and hereafter,  $c$  is the speed of light,  $\lambda = c/f_0$  the wavelength, and  $(\forall \theta \in \mathbb{V}) \mathbf{a}_{M_t}(\theta) \in \mathbb{C}^{M_t}$ ,  $\mathbf{a}_{M_r}(\theta) \in \mathbb{C}^{M_r}$  are the TX and RX steering vectors. We assume enough proximity between TX and RX antennas to consider  $\bar{\mathbf{H}}_{\text{si}}(n)$  an instantaneous flat-fading channel,  $\bar{\mathbf{H}}_{\text{si}}(n) \approx \mathbf{H}_{\text{si}} \delta(n)$ ,  $\mathbf{H}_{\text{si}} \in \mathbb{C}^{M_r \times M_t}$ , and hence we can write the signal received by the transceiver as  $(\forall n \in [N])$

$$y_r(n) = \bar{y}_r(n) + w_r(n), \quad w_r(n) \sim \mathcal{CN}(0, \sigma_r^2), \quad (4)$$

$$\bar{y}_r(n) = \sum_{q \in [Q]} \alpha_q \mathbf{c}^H \mathbf{H}_r(\theta_q) \mathbf{w} s(n - n_q) + \mathbf{c}^H \mathbf{H}_{\text{si}} \mathbf{w} s(n).$$

Without loss of generality, we assume  $M := M_t = M_r$  and  $\mathbf{a}(\theta) := \mathbf{a}_{M_t}(\theta) = \mathbf{a}_{M_r}(\theta)$  to ease the formulation in the remainder of the paper. We also note that the model can

be easily extended to incorporate the targets' velocities  $\nu_q$  by redefining the one-dimensional  $\delta(n - n_q)$  into a 2D delta in the delay-Doppler plane,  $\delta'(n - n_q, \nu - \nu_q)$  [17]. Likewise, bidirectional communication can be accommodated through time division, for which the transceiver's RX beamformer can be optimized in a completely decoupled way.

## II. PROBLEM FORMULATION

The objective of the proposed algorithm is the design of the analog beamforming vectors  $\mathbf{w}$  and  $\mathbf{c}$  that optimize (in a well-defined sense) the ISAC operation of the transceiver in Fig. 1. To this end, we must take into account the power limitations  $P_{\text{ant}}$ ,  $P_{\text{sat}}$  from Section I-B, and also impose SI-suppression capabilities,  $\mathbf{c}^H \mathbf{H}_{\text{si}} \mathbf{w} \simeq 0$ . Moreover, we need to incorporate the inequalities in (2) to ensure the desired communication performance. However, we first need to define a notion of sensing performance for which  $\mathbf{w}$  and  $\mathbf{c}$  can be optimized.

### A. Analog Beamforming and Radar Sensing

As mentioned in Section I, we address sensing through target detection rather than angle estimation. In the literature on ISAC beamforming, angle estimation is often approached by minimizing the MSE of  $\mathbf{W}$  either with respect to a desired covariance  $\mathbf{W}_*$  [14, 15], or to a beampattern  $p(\theta)$ ,  $p: \mathbb{V} \rightarrow \mathbb{R}_+ \cup \{0\}$  [13, 16], i.e.:

$$L_E(\mathbf{W}, \zeta) := \frac{1}{|\Theta_E|} \sum_{\theta \in \Theta_E} |\zeta p(\theta) - \mathbf{a}(\theta)^H \mathbf{W} \mathbf{a}(\theta)|^2. \quad (5)$$

Here,  $\zeta \in \mathbb{R}_+$  is an auxiliary optimization variable and  $\Theta_E \subset \mathbb{V}$  is a finite set of angle grid points. Alternatively, Liu et al. [18] directly optimize the Cramér-Rao bound for angle estimation under digital TX beamforming.

On the other hand, array-processing techniques are not available for analog beamforming, and the angle must be typically estimated through beam sweeping, possibly combined with a discovery/tracking scheme [17]. In this setup, the beam's main-lobe width  $\Delta\theta$  is the limiting factor for angle estimation, which is in turn mostly restricted by  $M$ .

Target detection offers more design freedom for  $\mathbf{w}$  and  $\mathbf{c}$ . In our multi-target scenario, we define an angular bin  $\Theta_b := [\theta_b - \Delta\theta/2, \theta_b + \Delta\theta/2] \subset \mathbb{V}$ , characterized by a central angle  $\theta_b$  and beam width  $\Delta\theta$ , to probe the presence of a target  $q_* \in [Q]$ . Noting that  $\{\theta_q\}_{q=1}^Q \cap \Theta_b = \{\theta_{q_*}\}$  and assuming SI cancellation in (4), we can pose the following hypothesis test:

$$\begin{aligned} H_0: y_r(n) &= \sum_{\substack{q \in [Q], \\ \theta_q \notin \Theta_b}} \alpha_q \mathbf{c}^H \mathbf{H}_r(\theta_q) \mathbf{w} \mathbf{s}(n - n_q) + w_r(n), \\ H_1: y_r(n) &= \sum_{q \in [Q]} \alpha_q \mathbf{c}^H \mathbf{H}_r(\theta_q) \mathbf{w} \mathbf{s}(n - n_q) + w_r(n), \end{aligned} \quad (6)$$

with unknown  $Q$ ,  $\alpha_q$ ,  $n_q$ , and  $\theta_q$ . A powerful test statistic for (6) is elusive due to the lack of knowledge on most parameters [19]. Luckily, we can design  $\mathbf{w}$  and  $\mathbf{c}$  such that

$$(\forall \theta \in \Theta_b)(\forall \vartheta \in \mathbb{V} \setminus \Theta_b) |\mathbf{c}^H \mathbf{H}_r(\theta) \mathbf{w}| \gg |\mathbf{c}^H \mathbf{H}_r(\vartheta) \mathbf{w}|. \quad (7)$$

In that case, we can approximate (6) as

$$\begin{aligned} H_0: y_r(n) &= w_r(n), \\ H_1: y_r(n) &= \alpha_{q_*} \mathbf{c}^H \mathbf{H}_r(\theta_{q_*}) \mathbf{w} \mathbf{s}(n - n_{q_*}) + w_r(n). \end{aligned} \quad (8)$$

We can now correlate  $y_r(n)$  with the known signal  $s(n)$  and apply the generalized likelihood ratio test [19] ( $\forall n \in \mathbb{Z} \setminus [N]$   $s(n) = 0$ ):

$$\frac{\max_{n' \in [N]} \left| \sum_{n \in [N]} y_r(n) s^*(n - n') \right|^2}{N \sigma_r^2 / 2} \underset{H_0}{\overset{H_1}{\geq}} \eta, \quad (9)$$

where  $\eta \in \mathbb{R}_+$  is a parameter that trades off the probability of false alarm  $P_{\text{FA}}$  and the probability of detection  $P_{\text{D}}$ . Specifically,  $P_{\text{FA}}$  and  $P_{\text{D}}$  are given by  $\chi_2^2$  and  $\chi_2^2(\rho)$ , the central and non-central chi distributions with two degrees of freedom, respectively, and  $\rho$  the non-centrality parameter

$$\rho = \frac{\alpha_{q_*}^2 N |\mathbf{c}^H \mathbf{H}_r(\theta_{q_*}) \mathbf{w}|^2}{\sigma_r^2 / 2}. \quad (10)$$

It is known that, for a fixed  $P_{\text{FA}}$ ,  $P_{\text{D}} =: f_{\text{D}}(\rho; P_{\text{FA}})$  is monotonically increasing in  $\rho$  [19]. In other words, we can design  $\mathbf{w}$  and  $\mathbf{c}$  to maximize  $P_{\text{D}}$  via (10) while enforcing (7), which leads to a low-SLL design as in [7].

### B. Optimization Problem Statement

Taking into account the previous discussion, we pose the following optimization problem:

$$\underset{\mathbf{w} \in \mathbb{C}^M, \mathbf{c} \in \mathbb{C}^M}{\text{maximize}} \quad \min_{\theta \in \Theta_L} |\mathbf{c}^H \mathbf{H}_r(\theta) \mathbf{w}| \quad \text{s.t.} \quad (11a)$$

$$(\forall (\theta, \vartheta) \in \Theta_L \times \Theta_S) |\mathbf{c}^H \mathbf{H}_r(\theta) \mathbf{w}| \geq \gamma_s |\mathbf{c}^H \mathbf{H}_r(\vartheta) \mathbf{w}| \quad (11b)$$

$$\mathbf{c}^H \mathbf{H}_{\text{si}} \mathbf{w} = 0 \quad (11c)$$

$$(\forall k \in [K]) \quad \frac{|\mathbf{h}_k^H \mathbf{w}|^2}{\sigma_k^2} \geq \Gamma_k \quad (11d)$$

$$(\forall m \in [M]) \quad \mathbf{e}_m^H \mathbf{w} \mathbf{w}^H \mathbf{e}_m \leq P_{\text{ant}} \quad (11e)$$

$$(\forall m \in [M]) \quad \mathbf{g}_m^H \mathbf{w} \mathbf{w}^H \mathbf{g}_m \leq P_{\text{sat}} \quad (11f)$$

$$\|\mathbf{c}\| = 1, \quad (11g)$$

where  $\Theta_L := \{\theta_1, \dots, \theta_I\} \subset \Theta_b$  and  $\Theta_S := \{\vartheta_1, \dots, \vartheta_J\} \subset \mathbb{V} \setminus \Theta_b$  are two finite sets of angle points in the main lobe and sidelobes, respectively,  $\mathbf{g}_m := \mathbf{H}_{\text{si}}^H \mathbf{e}_m$ , and  $\gamma_s$  is a target SLL. We note that (11b) enforces (7) under proper  $\gamma_s$ ,  $\Theta_L$  and  $\Theta_S$ , in which case (11a) approximates optimal multi-target detection via (10). Moreover, the SI-suppression and SNR requirements are imposed by (11c) and (11d), while (11e) and (11f) impose the antenna power limitations due to  $P_{\text{ant}}$  and  $P_{\text{sat}}$ .

The joint problem (11) is a nonconvex quadratically constrained quadratic program and thus NP-hard [10]. In particular, the coupling of  $\mathbf{w}$  and  $\mathbf{c}$  in (11a)–(11c) renders the optimization problem difficult to solve. We suggest thus splitting (11) into two parallel optimization problems for TX and RX. For this, we first use the singular value decomposition of  $\mathbf{H}_{\text{si}} = \mathbf{U} \mathbf{S} \mathbf{V}^H$  to write:

$$\mathbf{H}_{\text{si}} = \mathbf{H}_U \mathbf{H}_V, \quad \mathbf{H}_U := \mathbf{U} \mathbf{S}^{1/2}, \quad \mathbf{H}_V := \mathbf{S}^{1/2} \mathbf{V}^H, \quad (12)$$

$$\mathbf{S}^{1/2} := \text{diag}(\sqrt{[\mathbf{S}]_{1,1}}, \dots, \sqrt{[\mathbf{S}]_{M,M}}).$$

Additionally, we recall (3b) to note that

$$(\forall \theta \in \mathbb{V}) \quad |\mathbf{c}^H \mathbf{H}_r(\theta) \mathbf{w}| = |\mathbf{c}^H \mathbf{a}(\theta)| |\mathbf{a}^H(\theta) \mathbf{w}|, \quad (13)$$

and hence we write the two separate problems (14) and (15):

$$\text{maximize}_{\mathbf{w} \in \mathbb{C}^M} \min_{\theta \in \Theta_L} |\mathbf{a}^H(\theta) \mathbf{w}| \quad \text{s.t.} \quad (14a)$$

$$(\forall (\theta, \vartheta) \in \Theta_L \times \Theta_S) \quad |\mathbf{a}^H(\theta) \mathbf{w}| \geq \sqrt{\gamma_s} |\mathbf{a}^H(\vartheta) \mathbf{w}| \quad (14b)$$

$$\|\mathbf{H}_V \mathbf{w}\| = 0 \quad (14c)$$

$$\text{Eqs. (11d)–(11f)} \quad (14d)$$

$$\text{and} \quad \text{maximize}_{\mathbf{c} \in \mathbb{C}^M} \min_{\theta \in \Theta_L} |\mathbf{c}^H \mathbf{a}(\theta)| \quad \text{s.t.} \quad (15a)$$

$$(\forall (\theta, \vartheta) \in \Theta_L \times \Theta_S) \quad |\mathbf{c}^H \mathbf{a}(\theta)| \geq \sqrt{\gamma_s} |\mathbf{c}^H \mathbf{a}(\vartheta)| \quad (15b)$$

$$\|\mathbf{c}^H \mathbf{H}_U\| = 0 \quad (15c)$$

$$\|\mathbf{c}\| = 1. \quad (15d)$$

Let us write  $\mathcal{F}_j \subset \mathbb{C}^M \times \mathbb{C}^M$  for the feasible region of (11), and  $(\mathbf{w}_*, \mathbf{c}_*)$  for a solution of (14)–(15). It is clear that (14c) & (15c) imply (11c), and (14b) & (15b) imply (11b), so that  $(\mathbf{w}_*, \mathbf{c}_*) \in \mathcal{F}_{t,r} \subset \mathcal{F}_j$ . It can also be proven that  $(\mathbf{w}_*, \mathbf{c}_*)$ , is a solution of (11a) in  $\mathcal{F}_{t,r}$  if the following condition holds:

$$\arg \min_{\theta \in \Theta_L} |\mathbf{a}^H(\theta) \mathbf{w}_*| = \arg \min_{\theta \in \Theta_L} |\mathbf{c}_*^H \mathbf{a}(\theta)|. \quad (16)$$

### C. Superiorized Projections in Hilbert Spaces

While (14) and (15) are still nonconvex, we can use the trace identity  $\text{tr}(\mathbf{A}\mathbf{B}) = \text{tr}(\mathbf{B}\mathbf{A})$  and its particularization  $\text{tr}(\mathbf{v}\mathbf{v}^H) = \mathbf{v}^H \mathbf{v}$  to obtain semidefinite reformulations [10, 14–16]. That is, we define  $(\forall \theta \in \mathbb{V}) \mathbf{A}_\theta := \mathbf{a}(\theta) \mathbf{a}^H(\theta)$ , square (14a)–(14c) and (15a)–(15d), rearrange, and rewrite (14) and (15) as

$$\text{maximize}_{\mathbf{W} \in \mathbb{H}^M} \min_{\theta \in \Theta_L} \text{tr}(\mathbf{A}_\theta \mathbf{W}) \quad \text{s.t.} \quad (17a)$$

$$(\forall (\theta, \vartheta) \in \Theta_L \times \Theta_S) \quad \text{tr}((\mathbf{A}_\theta - \gamma_s \mathbf{A}_{\vartheta}) \mathbf{W}) \geq 0 \quad (17b)$$

$$\text{tr}(\mathbf{H}_V^H \mathbf{H}_V \mathbf{W}) = 0 \quad (17c)$$

$$(\forall k \in [K]) \quad \text{tr}(\mathbf{h}_k \mathbf{h}_k^H \mathbf{W}) \geq \sigma_k^2 \Gamma_k \quad (17d)$$

$$(\forall m \in [M]) \quad \text{tr}(\mathbf{e}_m \mathbf{e}_m^H \mathbf{W}) \leq P_{\text{ant}} \quad (17e)$$

$$(\forall m \in [M]) \quad \text{tr}(\mathbf{g}_m \mathbf{g}_m^H \mathbf{W}) \leq P_{\text{sat}} \quad (17f)$$

$$\mathbf{W} \succeq \mathbf{0} \quad (17g)$$

$$\text{rank}(\mathbf{W}) \leq 1 \quad (17h)$$

$$\text{maximize}_{\mathbf{C} \in \mathbb{H}^M} \min_{\theta \in \Theta_L} \text{tr}(\mathbf{A}_\theta \mathbf{C}) \quad \text{s.t.} \quad (18a)$$

$$(\forall (\theta, \vartheta) \in \Theta_L \times \Theta_S) \quad \text{tr}((\mathbf{A}_\theta - \gamma_s \mathbf{A}_{\vartheta}) \mathbf{C}) \geq 0 \quad (18b)$$

$$\text{tr}(\mathbf{H}_U \mathbf{H}_U^H \mathbf{C}) = 0 \quad (18c)$$

$$\text{tr}(\mathbf{C}) = 1 \quad (18d)$$

$$\mathbf{C} \succeq \mathbf{0} \quad (18e)$$

$$\text{rank}(\mathbf{C}) \leq 1. \quad (18f)$$

The optimization constraints  $\mathbf{W}, \mathbf{C}$  belong now to the Hilbert space  $\mathcal{H}$ , and the objective functions are minima of linear expressions, so that (17a) and (18a) maximize concave functions. Moreover, (17h) and (18f) represent the closed set

$\mathcal{R} := \{\mathbf{X} \in \mathcal{H} \mid \text{rank}(\mathbf{X}) \leq 1\}$ , the only nonconvex constraint, while (17b)–(17g) and (18b)–(18e) represent closed convex sets in  $\mathcal{H}$   $(\forall (\theta, \vartheta) \in \Theta_L \times \Theta_S)$   $(\forall k \in [K])$   $(\forall m \in [M])$ :

$$\mathcal{V} := \{\mathbf{X} \in \mathcal{H} \mid \langle \mathbf{H}_V^H \mathbf{H}_V, \mathbf{X} \rangle = 0\}, \quad (19a)$$

$$\mathcal{N}_k := \{\mathbf{X} \in \mathcal{H} \mid \langle \mathbf{h}_k \mathbf{h}_k^H, \mathbf{X} \rangle \geq \sigma_k^2 \Gamma_k\}, \quad (19b)$$

$$\mathcal{A}_m := \{\mathbf{X} \in \mathcal{H} \mid \langle \mathbf{e}_m \mathbf{e}_m^H, \mathbf{X} \rangle \leq P_{\text{ant}}\}, \quad (19c)$$

$$\mathcal{S}_m := \{\mathbf{X} \in \mathcal{H} \mid \langle \mathbf{g}_m \mathbf{g}_m^H, \mathbf{X} \rangle \leq P_{\text{sat}}\}, \quad (19d)$$

$$\mathcal{L}_{(\theta, \vartheta)} := \{\mathbf{X} \in \mathcal{H} \mid \langle \mathbf{A}_\theta - \gamma_s \mathbf{A}_{\vartheta}, \mathbf{X} \rangle \geq 0\}, \quad (19e)$$

$$\mathcal{P} := \{\mathbf{X} \in \mathcal{H} \mid \mathbf{X} \succeq \mathbf{0}\}, \quad (19f)$$

$$\mathcal{U} := \{\mathbf{X} \in \mathcal{H} \mid \langle \mathbf{H}_U \mathbf{H}_U^H, \mathbf{X} \rangle = 0\}, \quad (19g)$$

$$\mathcal{I} := \{\mathbf{X} \in \mathcal{H} \mid \langle \mathbf{I}, \mathbf{X} \rangle = 1\}. \quad (19h)$$

In order to find solutions to (17) and (18), we first drop the objective functions and rank constraints to consider the following convex feasibility problems:

$$\text{Find } \mathbf{W} \in \mathcal{H} \text{ such that } \mathbf{W} \text{ in (19a)–(19f),} \quad (20)$$

$$\text{Find } \mathbf{C} \in \mathcal{H} \text{ such that } \mathbf{C} \text{ in (19e)–(19h).} \quad (21)$$

Then, we approximate a solution to (20) and (21) through iterative sequential projections, where we only use two distinct relaxation parameters  $\mu, \mu'$  for simplicity:

$$(\forall i \in \mathbb{N}) \quad \mathbf{W}_{i+1} = T_T(\mathbf{W}_i) \quad (22)$$

$$:= T_{\mathcal{P}}^{\mu'} T_{\mathcal{V}}^{\mu'} T_{\mathcal{N}_{K \leftarrow 1}}^{\mu} T_{\mathcal{L}_{\theta_i \leftarrow \theta_1}}^{\mu} T_{\mathcal{S}_{M \leftarrow 1}}^{\mu} T_{\mathcal{A}_{M \leftarrow 1}}^{\mu}(\mathbf{W}_i)$$

$$(\forall i \in \mathbb{N}) \quad \mathbf{C}_{i+1} = T_R(\mathbf{C}_i) \quad (23)$$

$$:= T_{\mathcal{P}}^{\mu'} T_{\mathcal{U}}^{\mu'} T_{\mathcal{I}}^{\mu'} T_{\mathcal{L}_{(\theta_i, \vartheta_j)}}^{\mu} \dots T_{\mathcal{L}_{(\theta_1, \vartheta_1)}}^{\mu}(\mathbf{C}_i).$$

The mathematical expressions of the projections can be found in [10, 12]. It has been shown in [10, 20] that the mappings  $T_T$  and  $T_R$  are *bounded perturbation resilient*, i.e., they generate sequences converging to solutions of the convex feasibility problems in (20) and (21), even if bounded perturbations are added to their iterates. This enables us to use the iterations in (22) and (23) as *basic algorithms* for superiorization. By adding a sequence of well-designed bounded perturbations<sup>1</sup>  $(\beta_i \mathbf{v}_i)_{i \in \mathbb{N}}$  to the iterates of a basic algorithm  $\mathbf{x}_{i+1} = T(\mathbf{x}_i)$ ,  $\mathbf{x}_i \in \mathcal{H}$ , the superiorization methodology [11] automatically produces its *superiorized version*  $\mathbf{x}_{i+1} = T(\mathbf{x}_i + \beta_i \mathbf{v}_i)$ ,  $\mathbf{x}_i \in \mathcal{H}$ , which aims to find feasible points that are superior in a specified sense. Hence, the sequences produced by superiorized versions of the iterations in (22) and (23) are guaranteed to converge to solutions to (20) and (21), respectively.

In the following, we devise a sequence of perturbations to increase the objective value in (17a) and (18a), while simultaneously reducing the distance to the rank-constraint set  $\mathcal{R}$ . For this, we borrow from [9, Eq. (15)] the perturbation  $\mathcal{K}(\mathbf{X}) := P_{\mathcal{R}}(\mathbf{X}) - \mathbf{X}$ , where  $P_{\mathcal{R}}(\mathbf{X})$  is a projection onto  $\mathcal{R}$ ,

<sup>1</sup>See [21] for a formal definition of bounded perturbations.

and we conceive the perturbation  $\mathcal{Y}(\mathbf{X})$  for the supergradients of the objective functions:

$$\mathcal{Y}(\mathbf{X}) := (v_{\bar{\theta}} - v_{\underline{\theta}}) \frac{\mathbf{A}_{\theta}}{\|\mathbf{A}_{\theta}\|_{\mathcal{H}}}, \quad v_{\theta} := \frac{\langle \mathbf{A}_{\theta}, \mathbf{X} \rangle}{\|\mathbf{A}_{\theta}\|_{\mathcal{H}}}, \quad (24)$$

$$\bar{\theta} \in \arg \max_{\theta \in \Theta_L} v_{\theta}, \quad \underline{\theta} \in \arg \min_{\theta \in \Theta_L} v_{\theta}.$$

In words,  $\mathcal{Y}(\mathbf{W})$  and  $\mathcal{Y}(\mathbf{C})$  increase the smallest term inside (17a) and (18a), respectively, up to the largest one. Since (17a) and (18a) are proportional to  $\|\mathbf{W}\|_{\mathcal{H}}$  and  $\|\mathbf{C}\|_{\mathcal{H}}$ , we should ensure that  $\mathbf{W}$  and  $\mathbf{C}$  reach their maximum feasible norms. Noting that (18d) already fixes  $\|\mathbf{C}\|_{\mathcal{H}}$ , we add a scale perturbation just for  $\mathbf{W}$ :

$$\mathcal{B}(\mathbf{W}) := (\beta - 1) \mathbf{W}, \quad (25)$$

$$\beta := \min \left( \min_{m \in [M]} \frac{P_{\text{ant}}}{\langle \mathbf{e}_m \mathbf{e}_m^H, \mathbf{W} \rangle}, \min_{m \in [M]} \frac{P_{\text{sat}}}{\langle \mathbf{g}_m \mathbf{g}_m^H, \mathbf{W} \rangle} \right).$$

The final algorithm iterations are as follows:

$$\begin{aligned} \mathbf{W}_{i+1} &= T_{\mathbf{T}}(\mathbf{W}_i + c_1^i \mathcal{K}(\mathbf{W}_i) + c_2^i \mathcal{Y}(\mathbf{W}_i) + c_3^i \mathcal{B}(\mathbf{W}_i)) \\ \mathbf{C}_{i+1} &= T_{\mathbf{R}}(\mathbf{C}_i + c_1^i \mathcal{K}(\mathbf{C}_i) + c_2^i \mathcal{Y}(\mathbf{C}_i)), \end{aligned} \quad (26)$$

with  $a_1, a_2, a_3 \in (0, 1)$  the decaying coefficients of the perturbations. Since (26) is guaranteed to converge, we set the stop condition  $\|\mathbf{X}_{i+1} - \mathbf{X}_i\|_{\mathcal{H}} < \epsilon \|\mathbf{X}_{i+1}\|_{\mathcal{H}}$  and extract  $(\mathbf{w}_*, \mathbf{c}_*)$  as the largest principal component from  $\mathbf{W}_i$  and  $\mathbf{C}_i$ .

### III. NUMERICAL RESULTS

For the simulations, we choose  $f_0 = 28$  GHz and  $\lambda/2$ -spaced uniform linear arrays (ULAs) with  $P_{\text{ant}} = 10$  dBm,  $P_{\text{sat}} = -20$  dBm, and  $M_t = M_r = 10$ , so that  $\mathbb{V} = [-\pi/2, \pi/2]$  and

$$\mathbf{a}(\theta) = \left[ 1, e^{j\pi \sin \theta}, \dots, e^{j\pi(M-1) \sin \theta} \right]^T, \quad M = 10. \quad (27)$$

Moreover, we assume that the TX and RX arrays constitute the left and right subarrays of a  $\lambda/2$ -ULA of size  $M_t + M_r$  and total length 10.2 cm, for which we model  $\mathbf{H}_{\text{si}}$  as:

$$[\mathbf{H}_{\text{si}}]_{m',m} = \varrho(d_{m',m}) \exp(2\pi d_{m',m}/\lambda), \quad (28)$$

where  $d_{m',m}$  is the distance between TX and RX antennas  $m$  and  $m'$ , and  $\varrho(d)$  is Friis' path loss, which is a valid approximation for  $d_{m',m} \geq \lambda/2$  [22].

We consider  $(\forall q \in [Q]) \xi_q = 1 \text{ m}^2$ ,  $(\forall k \in [K]) \sigma_k^2 = \sigma_r^2 = -88$  dBm, and  $\Gamma_k = 3$  dB. We adopt the geometric fading channel model from [2] for  $\mathbf{h}_k$  with path-loss factor 2.2 and Rician factor  $\kappa = 1000$ .

#### A. Beamforming Analysis

We choose a beam at  $\theta_b = 0^\circ$  with  $\Delta\theta = 20^\circ$ , which gives  $\gamma_s \simeq 30$  dB according to Dolph-Chebyshev's minimum SLL for  $M = 10$ . [23]. We also leave a  $6^\circ$  guard band, so that  $\Theta_L$  spans  $-7^\circ$  to  $7^\circ$ , and  $\Theta_S$  spans  $\pm 13^\circ$  to  $\pm 90^\circ$ , in  $1^\circ$ -steps. For the superiorized projections onto convex sets (SPOCS), we set  $\mu' = 1$ ,  $\mu = 1.5$ ,  $\epsilon = 10^{-5}$ ,  $a_1 = a_3 = 0.9999$ , and  $a_2 = 0.99$ . We obtain  $\mathbf{w}_*$  for  $K = 2$  after 1000 iterations, where the users are located at  $\theta_1 = -25^\circ$ ,  $\theta_2 = 40^\circ$ , and  $r_k = 20$  m for  $k = 1, 2$ .

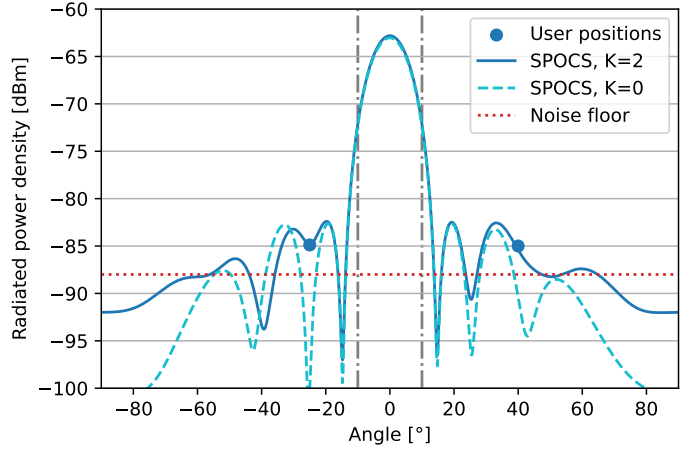


Fig. 2: TX angular power spectrum at  $r_k = 2$  m. The inclusion of  $K = 2$  users alters the sidelobes to guarantee their SNR.

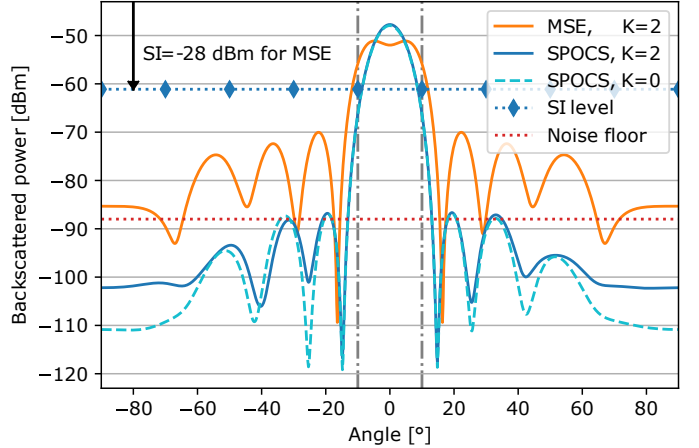


Fig. 3: Backscattered APS from target  $q_*$  at  $r_{q_*} = 2$  m. Our method decreases SLL by 20 dB and adds 33 dB SI attenuation compared to MSE.

Fig. 2 shows the angular power spectrum (APS) at  $r_k$  for  $K = 2$  and compares it with a useless case ( $K = 0$ ). The main beam and SLL are similar in both cases, but the SNR constraints in (2) shift and fill the beampattern's zeros for  $K = 2$ . In practice,  $\gamma_s$  needs to be selected carefully to avoid conflicts with the required SNRs  $\Gamma_k$ .

The overall effect of  $(\mathbf{w}_*, \mathbf{c}_*)$  is shown in Fig. 3 for a target  $q_*$  at  $r_{q_*} = 2$  m and arbitrary  $\theta_{q_*}$ . The joint beamforming fulfills (16) and attains an SI suppression below  $-60$  dBm, which leaves only 27 dB above the noise floor to be canceled digitally. We compare its APS with the baseline from [16]. For this, we set MSE minimization from (5) as the objective in (17) and (18) with  $\Theta_E = \Theta_L \cup \Theta_S$  and  $p(\theta) = 1$  for  $\theta \in \Theta_b$  and 0 elsewhere; we enforce (17e) with equality, we drop all SI and SLL constraints, and we obtain  $\mathbf{W}$  and  $\mathbf{P}$  with a standard convex solver. The MSE baseline yields an SI level of  $-28$  dBm, 33 dB above our method, which represents

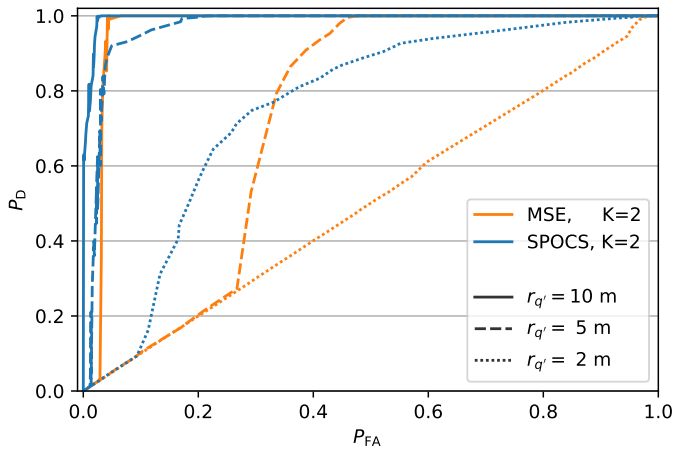


Fig. 4: ROC curves with  $r_{q_*} = 20$  m and unprobed target  $q'$ .

a reduction in the ADC's dynamic range equivalent to 5 bits. Moreover, the baseline's SLL lies 20 dB above that of SPOCS.

### B. Multi-target Detection

We investigate the impact of SLL on detection in a scenario with one probed and one unprobed target,  $q_*$  and  $q'$ , with  $r_{q_*} = 20$  m,  $r_{q'} \in \{2, 5, 10\}$  m,  $\theta_{q_*} \in \Theta_b$ , and  $\theta_{q'} \in \mathbb{V} \setminus \Theta_b$ . We estimate  $P_D$  and  $P_{FA}$  for  $(\mathbf{w}_*, \mathbf{c}_*)$  from (9), where we use 100 log-spaced values for  $\eta \in [5, 5 \times 10^6]$ , we run 5000 Monte Carlo simulations per  $\eta$  value, and we sample  $\theta_{q_*}$  and  $\theta_{q'}$  uniformly. The waveform of  $s(n)$  is single-carrier OFDM with QPSK modulation, 5G numerology 5, and 68 resource blocks; hence  $T = 2.23 \mu\text{s}$ ,  $N = 4384$ , and  $B_s = 391.7$  MHz.

According to the resulting receiver operating characteristic (ROC) curves in Fig. 4,  $r_{q'} = 10$  m has little impact on detection for both beampatterns, but MSE's performance sharply decreases for closer unprobed targets. Indeed, SPOCS achieves perfect  $P_D$  at  $r_{q'} = 5$  m for  $P_{FA} > 0.2$  in contrast to  $P_{FA} > 0.45$  for MSE. Furthermore,  $q'$  completely overshadows the MSE beampattern at 2 m, so that  $P_D \simeq P_{FA} \forall \eta$ , whereas SPOCS can still achieve modest  $P_D$  and  $P_{FA}$ .

## IV. CONCLUSIONS

In this paper, we have explored analog beamforming for SI-suppressed monostatic ISAC. We have identified target detection as the key performance parameter for analog beamforming, which has allowed us to formalize an optimization framework for sensing under communication constraints. In this sense, we have approached optimal ISAC through parallel TX and RX optimization via superiorized projections. Finally, we have shown through simulations how this approach outperforms a popular ISAC beamforming technique.

### ACKNOWLEDGMENT

The authors of this work acknowledge the financial support by the Federal Ministry of Education and Research of Germany (BMBF) in the programme "Souverän. Digital. Vernetzt." Joint project 6G-RIC (grant numbers: 16KISK020K, 16KISK030). Rodrigo Hernangómez acknowledges BMBF

support in the project "6G-ICAS4Mobility" (grant number: 16KISK235). Zoran Utkovski acknowledges BMBF support in the project "KOMSENS-6G" (grant number: 16KISK121).

### REFERENCES

- [1] F. Liu, Y. Cui, C. Masouros, J. Xu, T. X. Han, Y. C. Eldar, and S. Buzzi, "Integrated Sensing and Communications: Toward Dual-Functional Wireless Networks for 6G and Beyond," *IEEE J. Sel. Areas Commun.*, vol. 40, no. 6, pp. 1728–1767, Jun. 2022.
- [2] Z. Liu, S. Aditya, H. Li, and B. Clerckx, "Joint Transmit and Receive Beamforming Design in Full-Duplex Integrated Sensing and Communications," *IEEE J. Sel. Areas Commun.*, vol. 41, no. 9, pp. 2907–2919, Sep. 2023.
- [3] R. Askar, T. Kaiser, B. Schubert, T. Haustein, and W. Keusgen, "Active Self-Interference Cancellation Mechanism for Full-Duplex Wireless Transceivers," in *2014 9th Int. Conf. Cognitive Radio Oriented Wireless Netw., (CROWNCOM)*, Jun. 2014, pp. 539–544.
- [4] C. Baquero Barneto, E. Rastorgueva-Foi, M. F. Keskin, T. Riihonen, M. Turunen, J. Talvitie, H. Wymeersch, and M. Valkama, "Millimeter-Wave Mobile Sensing and Environment Mapping: Models, Algorithms and Validation," *IEEE Trans. Veh. Technol.*, vol. 71, no. 4, pp. 3900–3916, Apr. 2022.
- [5] T. Wild, A. Grudnitsky, S. Mandelli, M. Henninger, J. Guan, and F. Schaich, "6G Integrated Sensing, Communication: From Vision to Realization," *arXiv preprint arXiv:2305.01978*, 2023.
- [6] Z. He, W. Xu, H. Shen, D. W. K. Ng, Y. C. Eldar, and X. You, "Full-Duplex Communication for ISAC: Joint Beamforming and Power Optimization," *IEEE J. Sel. Areas Commun.*, vol. 41, no. 9, pp. 2920–2936, Sep. 2023.
- [7] A. Liu, T. Riihonen, and W. Sheng, "Full-Duplex Analog Beamforming Design for mm-Wave Integrated Sensing and Communication," in *2023 IEEE Radar Conf.* San Antonio, TX, USA: IEEE, May 2023, pp. 1–6.
- [8] J. Fink, R. L. G. Cavalcante, Z. Utkovski, and S. Stańczak, "A Set-Theoretic Approach to MIMO Detection," in *2022 IEEE Int. Conf. Acoust., Speech, Signal Process. (ICASSP)*, May 2022, pp. 5328–5332.
- [9] J. Fink, R. L. G. Cavalcante, and S. Stańczak, "Multicast Beamforming Using Semidefinite Relaxation and Bounded Perturbation Resilience," in *2019 IEEE Int. Conf. Acoust., Speech, Signal Process. (ICASSP)*, May 2019, pp. 4749–4753.
- [10] —, "Multi-Group Multicast Beamforming by Superiorized Projections Onto Convex Sets," *IEEE Trans. Signal Process.*, vol. 69, pp. 5708–5722, 2021.
- [11] Y. Censor, R. Davidi, and G. T. Herman, "Perturbation resilience and superiorization of iterative algorithms," *Inverse problems*, vol. 26, no. 6, p. 065008, 2010.
- [12] S. Theodoridis, K. Slavakis, and I. Yamada, "Adaptive Learning in a World of Projections," *IEEE Signal Process. Mag.*, vol. 28, no. 1, pp. 97–123, Jan. 2011.

- [13] P. Stoica, J. Li, and Y. Xie, "On Probing Signal Design For MIMO Radar," *IEEE Trans. Signal Process.*, vol. 55, no. 8, pp. 4151–4161, Aug. 2007.
- [14] F. Liu, C. Masouros, A. Li, H. Sun, and L. Hanzo, "MU-MIMO Communications With MIMO Radar: From Co-Existence to Joint Transmission," *IEEE Trans. Wireless Commun.*, vol. 17, no. 4, pp. 2755–2770, Apr. 2018.
- [15] F. Liu, L. Zhou, C. Masouros, A. Li, W. Luo, and A. Petropulu, "Toward Dual-functional Radar-Communication Systems: Optimal Waveform Design," *IEEE Trans. Signal Process.*, vol. 66, no. 16, pp. 4264–4279, Aug. 2018.
- [16] X. Liu, T. Huang, N. Shlezinger, Y. Liu, J. Zhou, and Y. C. Eldar, "Joint Transmit Beamforming for Multiuser MIMO Communications and MIMO Radar," *IEEE Trans. Signal Process.*, vol. 68, pp. 3929–3944, 2020.
- [17] S. K. Dehkordi, L. Gaudio, M. Kobayashi, G. Caire, and G. Colavolpe, "Beam-Space MIMO Radar for Joint Communication and Sensing with OTFS Modulation," *IEEE Trans. Wireless Commun.*, pp. 1–1, 2023.
- [18] F. Liu, Y.-F. Liu, A. Li, C. Masouros, and Y. C. Eldar, "Cramér-Rao Bound Optimization for Joint Radar-Communication Beamforming," *IEEE Trans. Signal Process.*, vol. 70, pp. 240–253, 2022.
- [19] S. M. Kay, *Fundamentals of statistical processing, Volume 2: Detection theory*. Pearson Education India, 2009.
- [20] H. He and H.-K. Xu, "Perturbation resilience and superiorization methodology of averaged mappings," *Inverse Problems*, vol. 33, no. 4, p. 044007, 2017.
- [21] Y. Censor, "Weak and strong superiorization: between feasibility-seeking and minimization," *arXiv preprint arXiv:1410.0130*, 2014.
- [22] H. Schantz, "Near field propagation law & a novel fundamental limit to antenna gain versus size," in *2005 IEEE Antennas, Propag. Soc. Int. Symp.*, vol. 3A, Jul. 2005, pp. 237–240 vol. 3A.
- [23] P. Lynch, "The Dolph–Chebyshev Window: A Simple Optimal Filter," *Monthly Weather Review*, vol. 125, no. 4, pp. 655–660, Apr. 1997.